

Hubble Tension and Dark Energy in Teleparallel Gauss-Bonnet Gravity: New Constraints from DESI BAO, Pantheon⁺ and Hubble Data

Santosh V. Lohakare,^{a,b} S. K. Maurya,^{a,1} Aaisha Al Qassabi,^a B. Mishra^d

^aDepartment of Mathematical and Physical Sciences, College of Arts and Sciences, University of Nizwa, P.O. Box 33, Nizwa 616, Sultanate of Oman

^bDepartment of Mathematics, School of Computer Science and Artificial Intelligence, SR University, Warangal-506371, Telangana, India

^dDepartment of Mathematics, Birla Institute of Technology and Science-Pilani, Hyderabad Campus, Jawahar Nagar, Kapra Mandal, Medchal District, Telangana 500078, India

E-mail: l.santoshvijay@sru.edu.in, sunil@unizwa.edu.om, aaishakhalifa@unizwa.edu.om, bivu@hyderabad.bits-pilani.ac.in

Abstract. We explore the cosmological dynamics of a teleparallel Gauss-Bonnet gravity model defined by the torsion scalar T and the torsion-based Gauss-Bonnet invariant $T_{\mathcal{G}}$, deriving modified Friedmann equations for a flat FLRW Universe and corresponding linear scalar perturbation equations. Using a numerical approach, we solve these equations for pressureless matter, predicting the redshift evolution of the Hubble parameter $H(z)$. Bayesian Markov chain Monte Carlo analysis, incorporating late-time observations from Cosmic Chronometers, Pantheon⁺ with SH0ES, and DESI BAO (Data Release 1 and Data Release 2), constrains the model parameters, revealing that $f(T, T_{\mathcal{G}})$ mimics dark energy in the absence of a cosmological constant, presenting a viable alternative to Λ CDM paradigm. Stability is confirmed via scalar perturbation analysis of Hubble and matter density fluctuations, positioning $f(T, T_{\mathcal{G}})$ gravity as a robust framework to address cosmic acceleration challenges. The model yields a present-day effective equation of state $\omega_{\text{eff}}(z=0) \approx -0.664$ to -0.693 , consistent with observations, and partially alleviates the Hubble tension with H_0 estimates of 69 to $71.5 \text{ km s}^{-1} \text{ Mpc}^{-1}$. These findings highlight the potential of $f(T, T_{\mathcal{G}})$ gravity to resolve fundamental cosmological puzzles while aligning with late-time observational data.

¹Corresponding author

Contents

1	Introduction	1
2	Mathematical Formalism of $f(T, T_G)$ Gravity	3
2.1	Numerical Results	6
3	Cosmological Observations with Numerical Approach	7
3.1	Cosmological datasets	7
3.1.1	Cosmic Chronometers (CC)	7
3.1.2	Supernovae type Ia (SNe Ia)	7
3.1.3	Baryon Acoustic Oscillation (BAO)	8
3.2	Statistical analysis	12
4	Perturbations and stability	14
5	Conclusion	18
6	BAO Distance Measurements from Observational Data	20

1 Introduction

Astronomical observations, including Type Ia Supernovae (SNe Ia) as standard candles [1–3], cosmic microwave background (CMB) temperature anisotropies [4–6], weak gravitational lensing [7–9], baryon acoustic oscillations (BAO), large-scale matter distribution [10–14], and high-redshift galaxy clustering [15], robustly confirm the accelerating expansion of the Universe. Within general relativity (GR), this acceleration is attributed to dark energy, often modeled as a cosmological constant (Λ) with a constant equation of state (EoS) parameter $\omega_\Lambda = -1$ [16], forming the basis of the Λ CDM model alongside cold dark matter (CDM). However, Λ CDM faces theoretical challenges like the fine-tuning and cosmic coincidence problems [17, 18], as well as observational tensions, such as the Hubble constant (H_0) discrepancy and the matter fluctuation amplitude (S_8) tension, though recent KiDS-Legacy results [19] suggest the latter is alleviated ($S_8 = 0.815^{+0.016}_{-0.021}$, 0.73σ from Planck) [20, 21], prompting exploration of alternatives like dynamic dark energy within GR or modified gravity theories [22–25]. Precise measurements of the dark energy EoS and its evolution remain critical to unraveling its nature [24, 26, 27].

Recent cosmological findings from the Dark Energy Spectroscopic Instrument (DESI) [28] have marked a transformative advancement in our understanding of cosmic evolution. The DESI Stage IV survey significantly refines cosmological constraints through precise measurements of galaxy clustering, quasar distributions, and Lyman- α forest observations across extensive sky coverage and redshift ranges. The first year of DESI observations has yielded robust measurements of both transverse comoving distances and Hubble rates, derived from a sample exceeding six million extragalactic objects, the largest collected for such analyses to date. Initial results from the DESI BAO data release one (DR1) demonstrate remarkable consistency with the flat Λ CDM paradigm, reporting a matter density parameter $\Omega_{m0} = 0.295 \pm 0.015$. When combined with Big Bang Nucleosynthesis priors and cosmic microwave background acoustic scale measurements, these data constrain the Hubble constant to

$H_0 = 68.52 \pm 0.62 \text{ km s}^{-1} \text{ Mpc}^{-1}$. Further integration with Planck CMB anisotropy data and ACT/Planck CMB lensing measurements yields even tighter constraints: $\Omega_{\text{m}0} = 0.307 \pm 0.005$ and $H_0 = 67.97 \pm 0.38 \text{ km s}^{-1} \text{ Mpc}^{-1}$ [28]. These groundbreaking results not only validate the current cosmological standard model but also provide an exceptionally precise observational foundation for testing alternative theories of cosmic acceleration and large-scale structure formation.

The phenomenon of late-time accelerated cosmic expansion has been extensively investigated through modifications to gravitational theory, offering an alternative to the dark energy paradigm. Within the framework of GR, such modifications are not feasible [29, 30]. To address this limitation, extensions to the geometrical structure of the Einstein-Hilbert action have been proposed to account for cosmic expansion. A prominent class of modified gravity theories emerges from extending the Einstein-Hilbert Lagrangian by incorporating additional curvature or matter-related terms. This generalized approach gives rise to several distinct formulations, including $f(R)$ (with R denoting the Ricci scalar), $f(T)$ (with T the torsion scalar), $f(Q)$ (with Q the non-metricity scalar), $f(\mathcal{G})$ (with \mathcal{G} the Gauss-Bonnet curvature term), and Lovelock gravity, among others (see [31–36]). These theoretical frameworks have garnered significant interest within the scientific community due to their rich and diverse cosmological implications, including their potential to address key challenges in modern cosmology such as late-time cosmic acceleration, Hubble tension and the nature of dark energy [37–42]. In the teleparallel formulation of gravity, higher curvature corrections, such as the Gauss-Bonnet invariant $T_{\mathcal{G}}$, can be incorporated, leading to actions that include higher torsion modifications [43–46]. Notably, the torsion-based Gauss-Bonnet invariant $T_{\mathcal{G}}$ has been derived without relying on the Weitzenböck connection, demonstrating equivalence to the Gauss-Bonnet term \mathcal{G} [47]. This development has given rise to a compelling class of modified gravitational theories, termed $f(T, T_{\mathcal{G}})$ gravity [47, 48].

Another avenue of modified gravity involves coupling the torsion scalar T with the trace of the energy-momentum tensor \mathcal{T} . This approach enables a unified description of cosmological phases, encompassing inflation, matter-dominated expansion, and late-time acceleration [49, 50]. Furthermore, extending $f(T)$ gravity by incorporating nonminimal torsion matter coupling into the action has proven effective in addressing the dark energy sector of the Universe [51]. This study focuses on a gravitational action combining the torsion scalar and the Gauss-Bonnet invariant, formulated within $f(T, T_{\mathcal{G}})$ gravity theories. These theories have been thoroughly explored across various contexts [48, 52, 53], yielding significant insights on multiple scales. The present research investigates the cosmological dynamics of a specific subclass of $f(T, T_{\mathcal{G}})$ models, selected based on symmetry considerations. The primary objective is to evaluate the viability of this scenario as an alternative to the standard cosmological paradigm using late-time cosmic observations. In this work, a numerical methodology has been developed to predict the redshift evolution of the Hubble expansion rate. The $f(T, T_{\mathcal{G}})$ model emerges as a promising candidate for explaining the current cosmological epochs, effectively capturing the evolution of energy components over cosmic time and reinforcing its potential as a viable explanation for the observed accelerated expansion of the Universe. To assess the model comprehensively, the background cosmological dynamics are analyzed, and its feasibility is evaluated through Bayesian inference, employing Markov chain Monte Carlo (MCMC) analysis. This analysis incorporates late-time observational datasets, including Supernovae Ia (Pantheon⁺), observational Hubble data (CC sample), DESI BAO Data Release 1 (DR1) and Data Release 2 (DR2) datasets. Additionally, a scalar perturbation analysis framework is introduced to examine the stability of the model. The results demonstrate that

the model robustly represents the evolving energy components across cosmic time, lending credence to its role as a compelling alternative explanation for the observed cosmic acceleration.

This study investigates the concept of an accelerating Universe through a novel, streamlined parameterization of the Hubble parameter within higher-order gravity theory, employing a numerical approach. The article is structured into five sections: Section 2 establishes the geometrical and mathematical foundation of teleparallelism, formulates $f(T, T_G)$ gravity, and derives the general metric and field equations. Section 3 applies this framework to a cosmological context, developing $f(T, T_G)$ cosmology supported by observational datasets. Section 4 builds on this model, conducting a scalar perturbation analysis to assess its stability. The article concludes in Section 5 with a summary of results and a discussion of the implications for cosmological modeling and potential future directions.

2 Mathematical Formalism of $f(T, T_G)$ Gravity

In the teleparallel formulation of gravity, the fundamental dynamical variables are the tetrad field $e_a(x^\mu)$ and the connection one-forms $\omega^a_b(x^\mu)$, which together define parallel transport. Here, Greek indices μ, ν, \dots denote spacetime coordinates, while Latin indices a, b, \dots refer to the tangent (Lorentz) space. These fields can be expressed in coordinate components as $e_a = e_a^\mu \partial_\mu$ and $\omega^a_b = \omega^a_{b\mu} dx^\mu = \omega^a_{bc} e^c$, where the dual tetrad is defined as $e^a = e^a_\mu dx^\mu$.

The commutation relations among the tetrad fields are given by

$$[e_a, e_b] = C^c_{ab} e_c, \quad (2.1)$$

where the structure functions C^c_{ab} are defined as

$$C^c_{ab} = e_a^\mu e_b^\nu (e^c_{\mu,\nu} - e^c_{\nu,\mu}), \quad (2.2)$$

with a comma indicating partial differentiation with respect to the coordinate.

We now define the torsion tensor in terms of tangent space components as

$$T^a_{bc} = \omega^a_{cb} - \omega^a_{bc} - C^a_{bc}, \quad (2.3)$$

and the curvature tensor is given by

$$R^a_{bcd} = \partial_c \omega^a_{bd} - \partial_d \omega^a_{bc} + \omega^e_{bd} \omega^a_{ec} - \omega^e_{bc} \omega^a_{ed} - C^e_{cd} \omega^a_{be}. \quad (2.4)$$

To establish orthonormality, we employ the spacetime metric g such that $g(e_a, e_b) = \eta_{ab}$, where $\eta_{ab} = \text{diag}(-1, 1, \dots, 1)$ denotes the Minkowski metric. This leads to the relation

$$g_{\mu\nu} = \eta_{ab} e^a_\mu e^b_\nu, \quad (2.5)$$

with Latin indices a, b, \dots raised and lowered using η_{ab} .

Finally, we introduce the contortion tensor, which captures the deviation from the Levi-Civita connection, defined as

$$\mathcal{K}_{abc} = \frac{1}{2} (T_{cab} - T_{bca} - T_{abc}) = -\mathcal{K}_{bac}. \quad (2.6)$$

We now impose the condition of teleparallelism, namely the vanishing of the curvature tensor, $R^a_{bcd} = 0$, which is required to hold in all frames. One way to satisfy this condition

is by adopting the Weitzenböck connection ($\tilde{\omega}_{\mu\nu}^\lambda$), which is defined purely in terms of the tetrad as

$$\tilde{\omega}_{\mu\nu}^\lambda = e_a^\lambda \partial_\nu e^a_\mu. \quad (2.7)$$

In the preferred frame (tangent-space components), this choice yields vanishing spin connection components: $\tilde{\omega}_{bc}^a = 0$.

The Ricci scalar R , constructed from the standard Levi-Civita connection, can be related to the torsion scalar T through the identity [54–56]

$$eR = -eT + 2\partial_\mu(eT_\nu^\mu), \quad (2.8)$$

where $e = \det(e_\mu^a) = \sqrt{|g|}$, and the torsion scalar T is defined by

$$T = \frac{1}{4}T^{\mu\nu\lambda}T_{\mu\nu\lambda} + \frac{1}{2}T^{\mu\nu\lambda}T_{\lambda\nu\mu} - T_{\nu\mu}^\nu T_\lambda^\lambda. \quad (2.9)$$

In $f(T, T_G)$ gravity [47, 48], the total modified gravitational action is given by

$$\mathcal{S} = \frac{1}{2\kappa^2} \int d^4x e f(T, T_G). \quad (2.10)$$

Having established the comparative metrics, we now turn to the theoretical foundations of our analysis. In this study, we explore a gravitational framework grounded in the torsion scalar T and the teleparallel Gauss-Bonnet invariant term T_G . This approach generalizes the teleparallel equivalent of general relativity (TEGR) by incorporating higher-order corrections through T_G , offering a compelling alternative to curvature-based modifications of gravity. We adopt the coupling constant $\kappa^2 = 8\pi G$, where G represents the Newtonian gravitational constant. In curvature-based gravity, the Gauss-Bonnet invariant is expressed as

$$\mathcal{G} \equiv R^2 - 4R^{ab}R_{ab} + R^{abcd}R_{abcd} \quad (2.11)$$

where R , R^{ab} , R^{abcd} denote the Ricci scalar, Ricci tensor, and Riemann tensor, respectively. In contrast, within the framework of torsion-based $f(T, T_G)$ gravity, the invariant T_G is defined as

$$T_G = \left(\mathcal{K}^{a_1}_{ea}\mathcal{K}^{ea_2}_b\mathcal{K}^{a_3}_{fc}\mathcal{K}^{fa_4}_d - 2\mathcal{K}^{a_1a_2}_a\mathcal{K}^{a_3}_{eb}\mathcal{K}^e_{fc}\mathcal{K}^{fa_4}_d + 2\mathcal{K}^{a_1a_2}_a\mathcal{K}^{a_3}_{eb}\mathcal{K}^{ea_4}_f\mathcal{K}^f_{cd} + 2\mathcal{K}^{a_1a_2}_a\mathcal{K}^{a_3}_{eb}\mathcal{K}^{ea_4}_{c,d} \right) \delta^{abcd}_{a_1a_2a_3a_4}. \quad (2.12)$$

where $\delta^{abcd}_{a_1a_2a_3a_4}$ is the generalized Kronecker delta. This formulation encapsulates the geometric structure of torsion-based gravity, facilitating the exploration of cosmological dynamics distinct from curvature-based approaches.

The gravitational field equations corresponding to the modified action (2.10) are derived with respect to the tetrad formulation

$$2(H^{[ac]b} + H^{[ac]b})_{,c} + 2(H^{[ac]b} + H^{[ba]c} - H^{[cb]a})\mathcal{C}^d_{dc} + (2H^{[ac]d} + H^{dca})\mathcal{C}^b_{cd} + 4H^{[db]c}\mathcal{C}_{(dc)}^a + T^a_{cd}H^{cdb} - h^{ab} + (f - Tf_T - T_G f_{T_G})\eta^{ab} = 0. \quad (2.13)$$

with

$$\begin{aligned}
H^{abc} = & f_T (\eta^{ac} \mathcal{K}^{bd}{}_d - \mathcal{K}^{bca} + f_{T_G} \left[\epsilon^{cprt} (2\epsilon^a{}_{dkf} \mathcal{K}^{bk}{}_p \mathcal{K}^d{}_{qr} + \epsilon_{qdkf} \mathcal{K}^{ak}{}_p \mathcal{K}^{bd}{}_r + \epsilon^{ab}{}_{kf} \mathcal{K}^k{}_{dp} \mathcal{K}^d{}_{qr}) \mathcal{K}^{qf}{}_t \right. \right. \\
& + \epsilon^{cprt} \epsilon^{ab}{}_{kd} \mathcal{K}^{fd}{}_p (\mathcal{K}^k{}_{fr,t} - \frac{1}{2} \mathcal{K}^k{}_{fq} \mathcal{C}^q{}_{tr}) + \epsilon^{cprt} \epsilon^{ak}{}_{df} \mathcal{K}^{df}{}_p (\mathcal{K}^b{}_{kr,t} - \frac{1}{2} \mathcal{K}^b{}_{kq} \mathcal{C}^q{}_{tr}) \left. \left. \right] \right. \\
& \left. + f_{T_G} \mathcal{C}^q{}_{pt} \mathcal{K}^{bk}{}_{[q} \mathcal{K}^{df}{}_{r]} + \epsilon^{cprt} \epsilon^a{}_{kdf} [(f_{T_G} \mathcal{K}^{bk}{}_p \mathcal{K}^{df}{}_r), t] \right] \tag{2.14}
\end{aligned}$$

and

$$h^{ab} = f_T \epsilon^a{}_{kcd} \epsilon^{bpqd} \mathcal{K}^k{}_{fp} \mathcal{K}^{fc}{}_q$$

where f_T and f_{T_G} represent the partial derivatives of f with respect to the torsion scalar T and the Gauss-Bonnet invariant T_G , respectively.

To derive the field equations of $f(T, T_G)$, we consider an isotropic and homogeneous Friedmann–Lemaître–Robertson–Walker (FLRW) spacetime, given by

$$ds^2 = -dt^2 + a^2(t)(dx^2 + dy^2 + dz^2), \tag{2.15}$$

where the scale factor $a(t)$ characterizes the uniform expansion of the Universe along spatial directions in a flat FLRW geometry. The diagonal tetrad for this spacetime is given by

$$e^a{}_\mu = \text{diag}(1, a(t), a(t), a(t)), \tag{2.16}$$

with a determinant $e = a^3(t)$. The dual tetrad is expressed as

$$e_\mu{}^a = \text{diag}(1, a^{-1}(t), a^{-1}(t), a^{-1}(t)). \tag{2.17}$$

In this context, the torsion scalar T and the teleparallel Gauss-Bonnet invariant T_G are formulated in terms of the Hubble parameter $H = \frac{\dot{a}(t)}{a(t)}$, where a dot denotes differentiation with respect to cosmic time t . Specifically, they are given by

$$T = 6H^2, \quad T_G = 24H^2(\dot{H} + H^2) \tag{2.18}$$

We further incorporate a matter action \mathcal{S}_m , corresponding to an energy-momentum tensor \mathcal{T}^{ab} , modeled as a perfect fluid with energy density ρ and pressure p . By varying the total action $\mathcal{S} + \mathcal{S}_m$, we derive the field equations in the FLRW geometry, as established by Kofinas et al. [48]

$$f - 12H^2 f_T - T_G f_{T_G} + 24H^3 \dot{f}_{T_G} = 2\kappa^2 \rho_m, \tag{2.19}$$

$$f - 4(\dot{H} + 3H^2)f_T - 4H\dot{f}_T - T_G f_{T_G} + \frac{2}{3H}T_G \dot{f}_{T_G} + 8H^2 \ddot{f}_{T_G} = -2\kappa^2 p_m. \tag{2.20}$$

with

$$f_T \equiv \frac{\partial f(T, T_G)}{\partial T}, \quad f_{T_G} \equiv \frac{\partial f(T, T_G)}{\partial T_G}. \tag{2.21}$$

Hereafter, we adopt the shorthand notation $f \equiv f(T, T_G)$ to streamline subsequent expressions. The standard matter density ρ_m is conserved independently, satisfying the continuity equation $\dot{\rho}_m + 3H(\rho_m + p_m) = 0$. To construct a physically viable cosmological model,

we compute the pressure p and energy density ρ for a suitable form of $f(T, T_G)$. The time derivatives of the partial derivatives are expressed as

$$\begin{aligned}\dot{f}_T &= f_{TT}\dot{T} + f_{TT_G}\dot{T}_G, \\ \dot{f}_{T_G} &= f_{TT_G}\dot{T} + f_{T_G T_G}\dot{T}_G, \\ \ddot{f}_{T_G} &= f_{TTT_G}\dot{T}^2 + 2f_{TT_G T_G}\dot{T}\dot{T}_G + f_{T_G T_G T_G}\dot{T}_G^2 + f_{TT_G}\ddot{T} + f_{T_G T_G}\ddot{T}_G,\end{aligned}$$

where f_{TT} , f_{TT_G} , and similar terms represent higher-order partial derivatives of $f(T, T_G)$ with respect to T and T_G . These expressions facilitate the analysis of cosmological evolution within the $f(T, T_G)$ gravity framework.

2.1 Numerical Results

The preceding analysis necessitates specifying the functional form of $f(T, T_G)$. In conventional $f(T)$ gravity, corrections typically involve powers of the torsion scalar T . However, in the context of $f(T, T_G)$ gravity, the teleparallel equivalent of the Gauss-Bonnet term T_G is of the same order as T^2 , since it includes quartic torsion contributions. Given that both T and $\sqrt{T^2 + \lambda_2 T_G}$ scale similarly, a consistent modified gravity framework must incorporate both. Consequently, a minimal yet non-trivial model that departs from GR without introducing a new mass scale is defined by

$$f(T, T_G) = -T + \alpha\sqrt{T^2 + \beta T_G}, \quad (2.22)$$

where α and β are dimensionless coupling parameters. This model, despite its simplicity, is capable of yielding rich and distinctive cosmological behavior, particularly relevant at late times, highlighting the potential and flexibility of $f(T, T_G)$ gravity [57, 58]. Notably, when $\beta = 0$, the theory reduces to the TEGR, which is equivalent to GR with a rescaled Newton's constant. The dynamical behavior of this case has been thoroughly investigated in the literature [59–61] for the condition $\beta = 0$. Therefore, in the following, we restrict our attention to scenarios where $\beta \neq 0$.

To derive the theoretical Hubble rate $H(z)$ for our model, we numerically solve the modified Friedmann equation (2.19). For the cosmological regime dominated by pressureless matter ($p_m = 0$), the energy density evolves as

$$\rho_m(z) = 3H_0^2\Omega_{m0}(1+z)^3, \quad (2.23)$$

where z is the cosmological redshift (defined via $a_0/a = 1+z$, with a_0 and a representing the present-day and emission-time scale factors, respectively), and Ω_{m0} denotes the current matter density parameter. Within this framework, the first Friedmann equation for our specific model takes the following form

$$\begin{aligned}-3H_0^2\Omega_{m0}(z+1)^3 + \frac{H^5}{((2\beta+3)H^4 - 2\beta(z+1)H^3H')^{3/2}} &\left(-\sqrt{3}\alpha\beta^2H(z+1)^2H'^2 \right. \\ &+ H\left((2\beta+3)\left(\sqrt{3}\alpha(\beta-3)H^2 - \sqrt{3}\alpha\beta^2H(z+1)^2H'' + 3\sqrt{H^3((2\beta+3)H - 2\beta(z+1)H')}\right)\right) \\ &\left. - \beta(z+1)H'\left(\sqrt{3}\alpha(\beta-9)H^2 + 6\sqrt{H^3((2\beta+3)H - 2\beta(z+1)H')}\right)\right) = 0,\end{aligned} \quad (2.24)$$

where the prime symbol ($'$) denotes differentiation with respect to the redshift parameter z . The second-order nonlinear differential equation (2.24) for $H(z)$ requires two boundary

conditions: (i) the present-day value $H(0) = H_0$, and (ii) the derivative constraint $H'(0) = \gamma$, where γ is optimized via MCMC analysis. This data-driven approach enables rigorous exploration of the parameter space while satisfying observational constraints. The Λ CDM model is characterized by the Hubble function, defined as

$$H_{\Lambda\text{CDM}} = H_0 \sqrt{1 - \Omega_{\text{m}0} + \Omega_{\text{DE}_0}}, \quad (2.25)$$

where Ω_{DE_0} representing the current value of the DE density parameter.

3 Cosmological Observations with Numerical Approach

We employ the `GetDist` library [62], a widely used toolkit for producing high-quality one and two-dimensional posterior distribution plots. The parameter space is explored through MCMC sampling with the `emcee` Python package [63]. The resulting chains are then analyzed with the `GetDist` Python interface [62] to extract parameter constraints and visualize the posterior distributions. We test the $f(T, T_G)$ model using three complementary late-time datasets: (1) Cosmic Chronometers (CC), which provide model-independent measurements of the Hubble parameter $H(z)$ through the differential age evolution of elliptical galaxies [64]; (2) the Pantheon⁺ samples without the SH0ES calibration (PPS), comprising 1701 SNe Ia extending up to redshift $0 \leq z \leq 2.3$ [65, 66]; and (3) BAO₁, DESI BAO DR1 and DESI BAO DR2, which offer precise distance measurements from galaxy clustering and Lyman- α forest observations over the redshift range $0.3 \leq z \leq 2.33$ [28, 67]. This multi-probe approach combines independent distance ladders (SNe Ia), expansion rate measurements (CC), and large-scale structure constraints (BAO), ensuring robust cosmological parameter estimation free from reference model assumptions [68–70]. The subsequent sections detail the distinctive features of each dataset and their corresponding likelihood functions, with particular emphasis on the improved precision offered by DESI DR2’s anisotropic clustering measurements compared to earlier BAO surveys.

3.1 Cosmological datasets

3.1.1 Cosmic Chronometers (CC)

The CC method provides a model-independent measurement of the Hubble parameter $H(z)$ by estimating the differential age evolution dt of passively evolving elliptical galaxies across small redshift intervals ($\delta z/z \leq 0.001$) [71]. This technique relies on high-precision spectroscopy of these “chronometers,” which formed simultaneously but are observed at slightly different redshifts, enabling a direct reconstruction of the expansion history of the Universe without cosmological assumptions. For our analysis, we employ the most recent CC dataset [64, 70], which incorporates a comprehensive covariance matrix to account for systematic uncertainties from stellar population synthesis models, including the initial mass function, stellar library, and metallicity dependencies. This approach builds upon earlier foundational work [72–74] while rigorously addressing both statistical and systematic errors to deliver robust $H(z)$ constraints.

3.1.2 Supernovae type Ia (SNe Ia)

SNe Ia are extremely bright stellar explosions that can be detected across the universe, even at redshifts as high as $z \sim 2.3$. They are widely regarded as premier cosmological distance indicators due to the remarkable homogeneity of their spectra and light curves, combined

with their widespread distribution across the sky. The distance modulus μ can be determined from SNe Ia observations using the relation

$$\mu = m_b - M, \quad (3.1)$$

where m_b is the apparent magnitude (serving as an overall flux normalization) and M is the absolute magnitude. Alternatively, μ can be expressed theoretically as

$$\mu = 25 + 5 \log_{10}(d_L(z)), \quad (3.2)$$

where $d_L(z)$ is the luminosity distance, defined as

$$d_L(z) = (1+z) \int_0^z \frac{c}{H(z')} dz', \quad (3.3)$$

and c is the speed of light in vacuum. The inclusion of PPS data, calibrated by SH0ES Cepheid observations, eliminates the need for an independent absolute magnitude calibration [75–78], allowing M to be treated as a free parameter. While recent studies have questioned aspects of these calibrations [79, 80], the methodology remains valid for cosmological constraints, as evidenced by robust weak lensing results [81, 82], BAO measurements [28], and SNe Ia distance calibrations [75].

3.1.3 Baryon Acoustic Oscillation (BAO)

BAO correspond to density fluctuations in baryonic matter, originating from acoustic density waves in the primordial plasma of the early Universe. The relevant measurements are documented in Ref. [28], which provides data and correlations for the comoving distance during the drag epoch, expressed as D_M/r_d , and the distance variable D_H/r_d . Here, r_d denotes the comoving sound horizon at the drag epoch, representing the maximum distance sound waves could propagate from the Big Bang until baryon decoupling. In cases with a low signal-to-noise ratio, the averaged quantity D_V/r_d is employed instead. It should be emphasized that when utilizing DESI BAO data alone, only the combined parameter $r_d H_0$ can be constrained. However, by combining DESI BAO measurements with complementary observational datasets, it becomes possible to independently determine r_d and the Hubble constant H_0 .

The BAO₁ observables listed in Table 3 and the statistics for the DESI samples used in the DESI DR1 and DR2 measurements as presented in Table 4 and 5, respectively (see Appendix B), are defined as follows

1. Hubble distance $D_H(z)$,

$$D_H(z) = \frac{c}{H(z)}. \quad (3.4)$$

2. Diameter angular distance $D_A(z)$,

$$D_A(z) = \frac{1}{(1+z)} \int_0^z \frac{c}{H(z')} dz'. \quad (3.5)$$

3. Transverse comoving distance $D_M(z)$,

$$D_M(z) = (1+z)D_A(z). \quad (3.6)$$

Datasets	H_0	Ω_{m0}	α	β	γ	M
CC+PPS	$71.411^{+1.214}_{-1.231}$	$0.291^{+0.021}_{-0.023}$	$1.301^{+0.051}_{-0.052}$	$-2.507^{+0.181}_{-0.180}$	$31.170^{+0.132}_{-0.132}$	$-19.291^{+0.080}_{-0.070}$
CC+PPS+BAO ₁	$70.168^{+0.850}_{-0.900}$	$0.322^{+0.018}_{-0.017}$	$1.211^{+0.042}_{-0.041}$	$-2.301^{+0.120}_{-0.130}$	$33.891^{+0.110}_{-0.120}$	$-19.351^{+0.070}_{-0.060}$
CC+PPS+DESI DR1	$70.456^{+1.000}_{-1.100}$	$0.316^{+0.020}_{-0.019}$	$1.257^{+0.045}_{-0.044}$	$-2.460^{+0.140}_{-0.150}$	$33.396^{+0.120}_{-0.125}$	$-19.224^{+0.060}_{-0.060}$
CC+PPS+DESI DR2	$69.144^{+0.450}_{-0.547}$	$0.307^{+0.021}_{-0.020}$	$1.189^{+0.038}_{-0.037}$	$-2.184^{+0.140}_{-0.130}$	$31.840^{+0.130}_{-0.120}$	$-19.378^{+0.070}_{-0.080}$

Table 1. Summary of MCMC-constrained cosmological parameters from the combined CC, PPS, and DESI BAO analysis. The table presents the posterior estimates for the Hubble constant (H_0), matter density parameter (Ω_{m0}), and modified gravity parameters (α , β , γ and M) with their 1σ confidence intervals.

4. Volume-averaged distance $D_V(z)$,

$$D_V(z) = \left[(1+z)^2 D_A^2(z) \frac{cz}{H(z)} \right]^{1/3}. \quad (3.7)$$

We analyze three distinct BAO datasets from various surveys: BAO₁ (see Table 3 in Appendix B), comprising 20 data points from SDSS [83–88], DES [89], and the WiggleZ Dark Energy Survey [90], and DESI DR1, consisting of 7 measurements from the DESI 2024 survey [28] and DESI DR2 2025 release [67]. Due to partial overlaps in sky regions and redshift ranges between DESI and prior surveys in BAO₁, these datasets should not be combined in a single statistical analysis, as correlations among shared objects, particularly at low redshifts, arise from differences in instrument performance and observing strategies, despite some agreement and ongoing discussions regarding inconsistencies, with DESI data considered more accurate due to enhanced fitting and data processing techniques. The dataset includes two isotropic BAO measurements: the Bright Galaxy Survey (BGS) at an effective redshift $z_{\text{eff}} = 0.30$ and quasars (QSO) at $z_{\text{eff}} = 1.49$, along with ten anisotropic BAO data points from the Luminous Red Galaxy (LRG) sample at $z_{\text{eff}} = 0.51$ and 0.71 , LRG+Emission Line Galaxy (ELG) at $z_{\text{eff}} = 0.93$, ELG alone at $z_{\text{eff}} = 1.32$, and Lyman- α quasars (Lya QSOs) at $z_{\text{eff}} = 2.33$. BAO, a powerful cosmological distance estimator, originates from pre-recombination density perturbations in the baryon-photon fluid, where gravitational potential wells drove acoustic waves that imprinted a characteristic scale in the large-scale structure. For enhanced precision, we also incorporate data from the DESI DR2 release [67], which offers improved measurements due to an expanded galaxy and quasar sample compared to DR1 [28]. A key advancement in DR2 is the ability to independently constrain the transverse comoving distance $D_M(z)$ and Hubble distance $D_H(z)$, whereas DR1 provided only the volume-averaged distance $D_V(z)$, highlighting the significance of the higher signal-to-noise ratio in the latest quasar dataset.

For the $f(T, T_G)$ gravity model investigated in this manuscript, we adopt the following prior ranges for the model parameters: $H_0 \in [50.0, 100.0] \text{ km s}^{-1} \text{ Mpc}^{-1}$, $\Omega_{m0} \in [0.01, 1.0]$, $\alpha \in [-5.0, 5.0]$, $\beta \in [-5.0, 5.0]$, $\gamma \in [0.0, 50.0]$, and $M \in [-20.0, -18.0]$. These priors are used in the MCMC analysis to constrain the model against observational datasets.

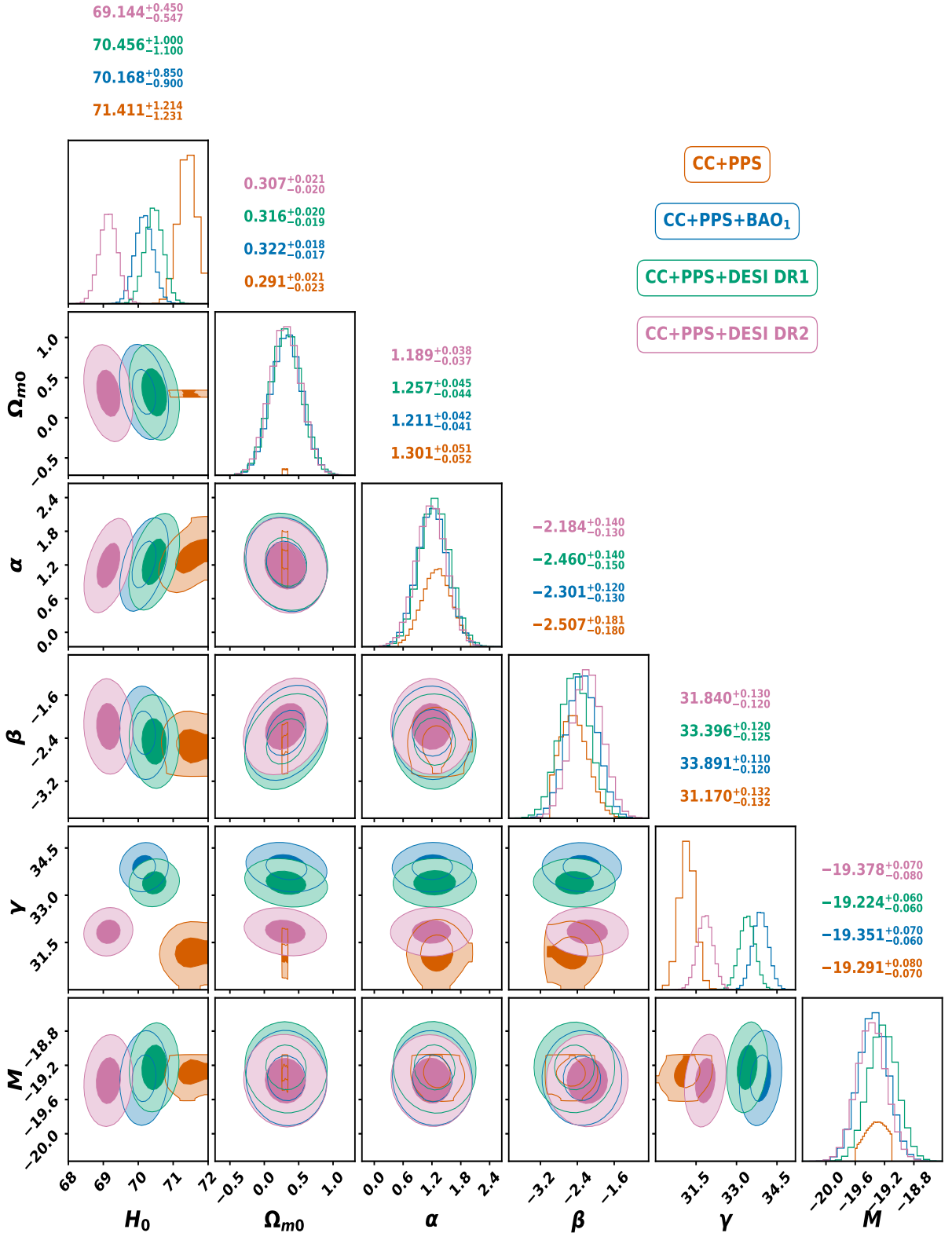


Figure 1. The contour plots display the 1σ and 2σ uncertainty regions for the model parameters H_0 , Ω_{m0} , α , β , γ and M . These contours are based on the combined CC+PPS, CC+PPS+BAO₁, CC+PPS+DESI DR1 and CC+PPS+DESI DR2 datasets.

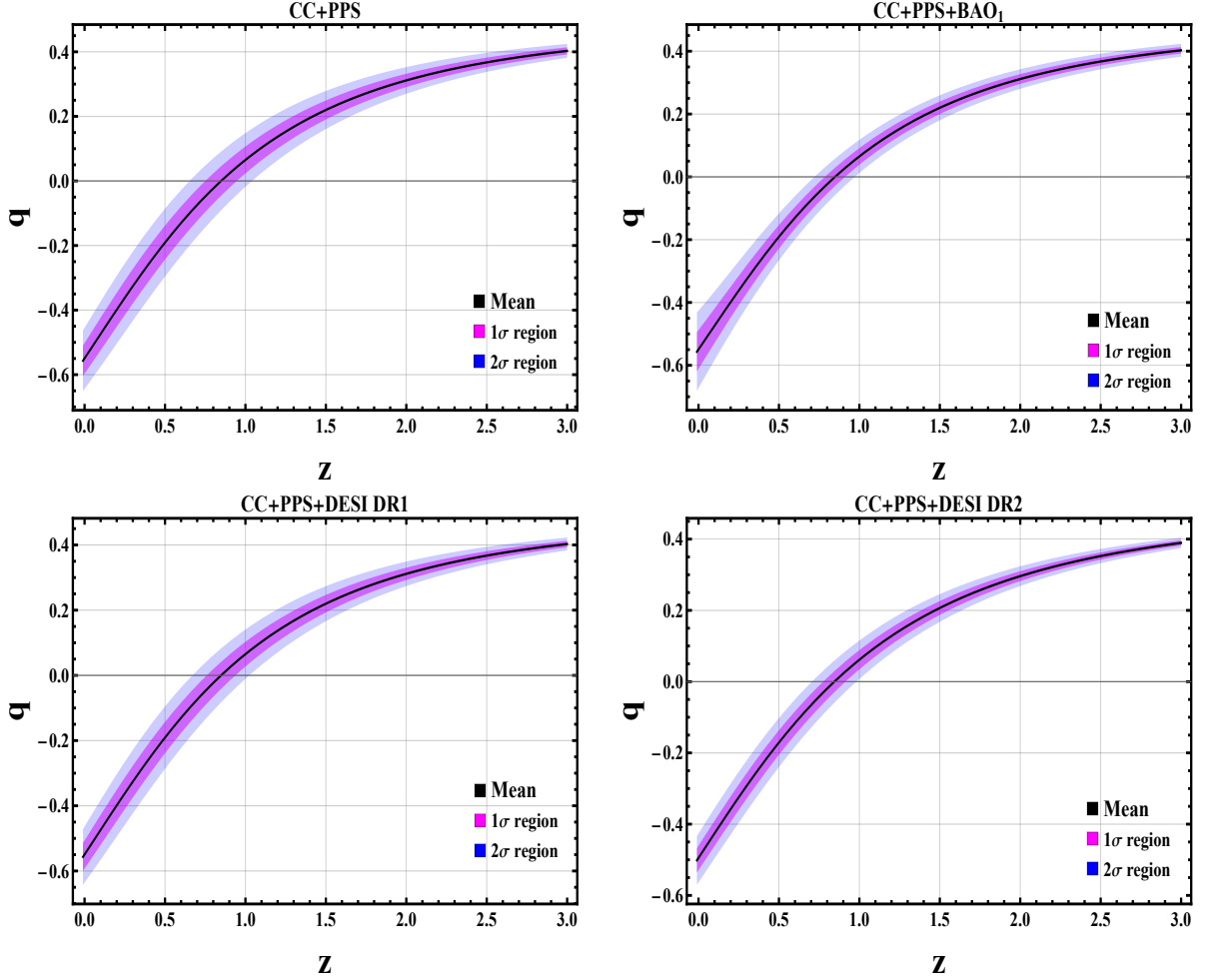


Figure 2. Behavior of the deceleration parameter using the combined datasets.

Figure 1 presents the 1σ (68% confidence) and 2σ (95% confidence) uncertainty regions for the parameters H_0 , $\Omega_{\text{m}0}$, α , β , γ and M , obtained through MCMC analysis. The contours compare constraints from four key datasets: CC+PPS, CC+PPS+BAO₁, CC+PPS+DESI DR1 and CC+PPS+DESI DR2 sample. Each pair of parameters shows marginalized posterior distributions, with the inner and outer contours delineating progressively tighter and broader confidence intervals, respectively. Figure 1 presents the constraints on the Hubble parameter H_0 derived from an MCMC analysis within the $f(T, T_G)$ gravity framework, utilizing various cosmological datasets. The best-fit values of H_0 are reported with their 68% confidence intervals, revealing a range of estimates such as $69.144^{+0.450}_{-0.547}$, $70.456^{+1.000}_{-1.100}$, $70.168^{+0.850}_{-0.900}$ and $71.411^{+1.214}_{-1.234}$. These results highlight the consistency of the $f(T, T_G)$ model across different datasets, with H_0 values clustering around $69\text{--}71.5 \text{ km s}^{-1} \text{ Mpc}^{-1}$, aligning closely with recent observational bounds. The tight constraints, particularly for datasets yielding $H_0 = 69.144^{+0.450}_{-0.547}$, underscore the model's robustness, while the slight variations across datasets reflect the influence of different observational priors. This analysis provides valuable insights into the viability of $f(T, T_G)$ gravity in describing late-time cosmic expansion, offering a pathway to address tensions in H_0 measurements.

Figure 2 highlights the critical role of the deceleration parameter $q = -1 + \frac{(1+z)H(z)H'(z)}{H(z)^2}$, a fundamental cosmological quantity that characterizes the expansion dynamics of the Universe. A positive value of q corresponds to a decelerating expansion, while a negative value indicates an accelerating phase. Analyzing the CC+PPS, CC+PPS+BAO₁, CC+PPS+DESI DR1, and CC+PPS+DESI DR2 datasets reveals a consistent evolution of q : it transitions from positive in the past signifying early deceleration to negative in the present, reflecting the current accelerated expansion, as shown in Figure 2. The present-day values of the deceleration parameter q_0 are found to be -0.549 , -0.538 , -0.549 , and -0.494 for the respective datasets. These estimates align well with the observational constraint $q_0 = -0.528^{+0.092}_{-0.088}$ reported by [91].

The model also indicates a smooth transition redshift, z_t , where the Universe shifted from deceleration to acceleration. The derived transition redshifts are $z_t = 0.834$, 0.842 , 0.846 , and 0.837 for the CC+PPS, CC+PPS+BAO₁, CC+PPS+DESI DR1, and CC+PPS+DESI DR2 datasets, respectively. These results are consistent with existing observational constraints, including $H(z)$ measurements at $z \approx 2.3$ from BAO data [92], and a transition redshift estimated as $z_t = 0.74 \pm 0.5$ [93], $z_t = 0.7679^{+0.1831}_{-0.1829}$ [94], and $z_t = 0.60^{+0.21}_{-0.12}$ [95].

Additionally, effective EoS parameter $\omega_{\text{eff}} = -1 + \frac{2(1+z)H(z)H'(z)}{3H(z)^2}$, plays a pivotal role in tracing the nature of the energy components driving cosmic acceleration. Figure 3, redshift evolution of the effective EoS parameter ω_{eff} for the $f(T, T_G)$ gravity model, derived from the CC+PPS, CC+PPS+BAO₁, CC+PPS+DESI DR1, and CC+PPS+DESI DR2 datasets. The present-day values range from -0.664 to -0.693 , consistent with a quintessence-like dark energy component. The slight steepening at low redshifts suggests a dynamic dark energy behavior, remaining above the phantom regime ($\omega_{\text{eff}} < -1$). These are consistent with previous constraints such as those from Planck 2018 [96] and from WMAP+CMB analyses [97]. The evolution of the effective EoS, derived from the computed energy density and pressure of dark energy, is also presented as a function of redshift in Figure 3.

3.2 Statistical analysis

We evaluate the performance of the model against the standard Λ CDM model using the Akaike Information Criterion (AIC) [98], the Bayesian Information Criterion (BIC) [99], and the minimum chi-squared statistic (χ^2_{min}). Both AIC and BIC balance the goodness of fit of a model with its complexity, determined by the number of parameters (n). The AIC is calculated as

$$\text{AIC} = \chi^2_{\text{min}} + 2n, \quad (3.8)$$

where χ^2 is derived from the value of the model's Gaussian likelihood function $\mathcal{L}(\hat{\theta} \mid \text{data})$, evaluated at the best-fit parameters. A lower AIC value indicates a better fit to the data, with a penalty applied to models with more parameters to account for overfitting. Similarly, the BIC is defined as

$$\text{BIC} = \chi^2_{\text{min}} + n \ln \mathcal{N}, \quad (3.9)$$

where \mathcal{N} is the number of data samples used in the MCMC process.

To compare the $f(T, T_G)$ model with the Λ CDM benchmark, we compute the differences in AIC and BIC, expressed as

$$\Delta\text{AIC} = \Delta\chi^2_{\text{min}} + 2\Delta n, \quad \Delta\text{BIC} = \Delta\chi^2_{\text{min}} + \Delta n \ln \mathcal{N}. \quad (3.10)$$

These metrics quantify deviations from the benchmark, with smaller ΔAIC and ΔBIC values indicating closer alignment with the Λ CDM model, suggesting superior model performance

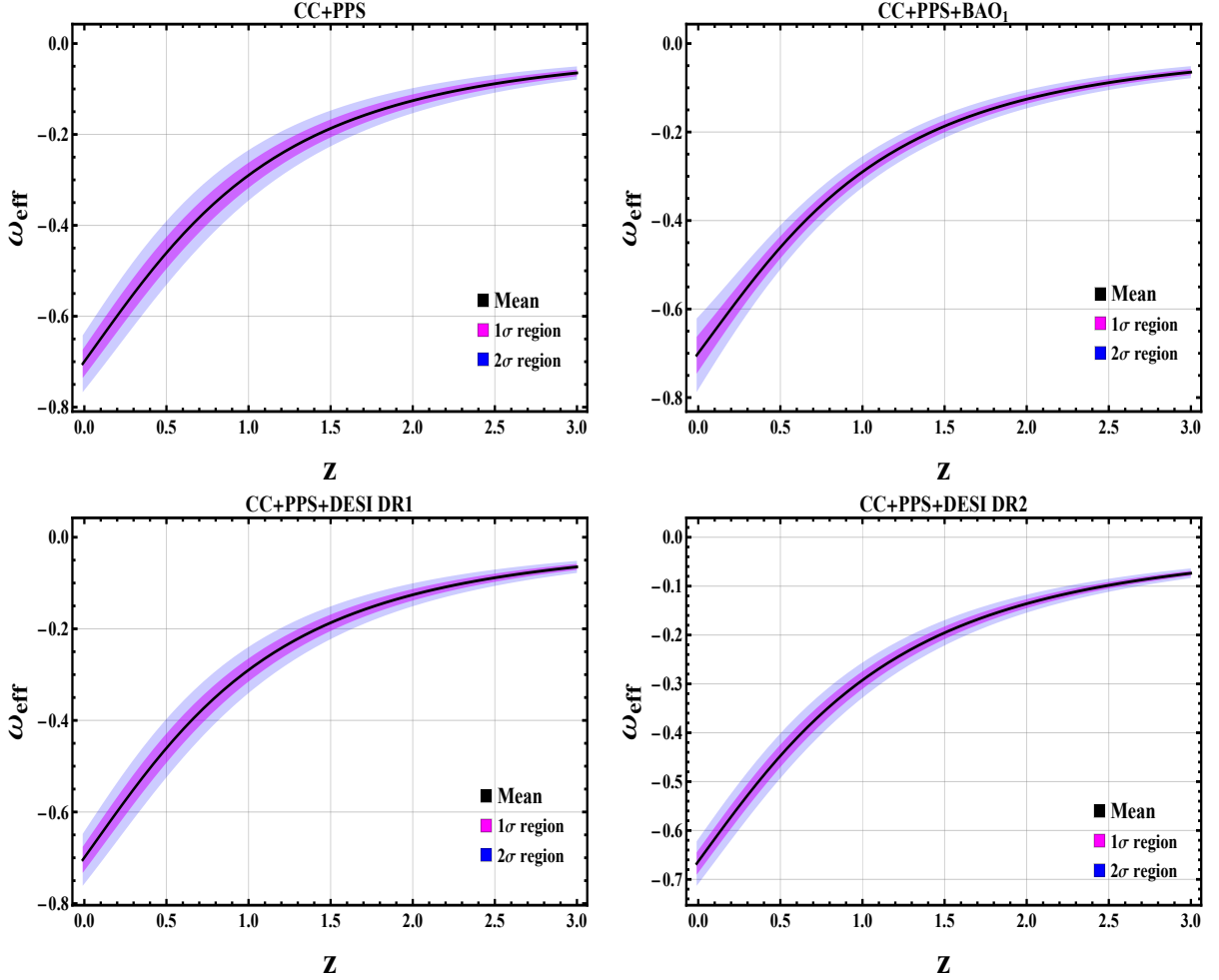


Figure 3. Behavior of the dark energy EoS parameter using the combined datasets.

Data sets	χ^2_{min}		AIC		BIC		ΔAIC	ΔBIC	\mathcal{N}
	$f(T, T_G)$	ΛCDM	$f(T, T_G)$	ΛCDM	$f(T, T_G)$	ΛCDM			
CC+PPS	1661.412	1682.482	36.132	1688.482	33.682	1704.855	-17.070	-6.155	$32+1701$
CC+PPS+BAO ₁	1676.329	1691.321	36.132	1697.321	33.682	1713.728	-10.992	-0.054	$32+1701+20$
CC+PPS+DESI DR1	1670.364	1688.234	36.132	1694.234	33.682	1710.619	-10.981	-0.055	$32+1701+7$
CC+PPS+DESI DR2	1671.238	1685.345	1628.774	1691.345	1634.924	1707.733	-12.996	-2.073	$32+1701+9$

Table 2. Goodness-of-fit statistics for the $f(T, T_G)$ gravity model: Minimum χ^2 values with corresponding ΔAIC and ΔBIC measures. The lower section compares this information criterion against the ΛCDM reference model, highlighting the relative performance of both cosmological scenarios.

relative to the dataset. This comparative analysis provides deeper insights into the consistency of each model with the standard cosmological framework.

Table 2 presents the goodness-of-fit statistics for the $f(T, T_G)$ gravity model, evaluated against the standard ΛCDM model, which assumes three free parameters. For ΛCDM , the minimum chi-squared (χ^2_{min}), AIC, and BIC values across the datasets are as follows: for CC+PPS, $\chi^2_{\text{min}} = 1682.482$, AIC = 1688.482, BIC = 1704.855; for CC+PPS+BAO₁, $\chi^2_{\text{min}} =$

1691.321, AIC = 1697.321, BIC = 1713.728; for CC+PPS+DESI DR1, $\chi^2_{\min} = 1688.234$, AIC = 1694.234, BIC = 1710.619; and for CC+PPS+DESI DR2, $\chi^2_{\min} = 1685.345$, AIC = 1691.345, BIC = 1707.733. These values serve as the reference for computing ΔAIC and ΔBIC for the $f(T, T_G)$ model. For the CC+PPS dataset, the $f(T, T_G)$ model yields $\chi^2_{\min} = 1661.412$, with $\Delta\text{AIC} = -17.070$ and $\Delta\text{BIC} = -6.155$, indicating a strong statistical preference over ΛCDM due to the significant negative values of both criteria. This suggests that the $f(T, T_G)$ model provides a better fit to the data despite its additional complexity. Similarly, for CC+PPS+DESI DR2, the $f(T, T_G)$ model achieves $\chi^2_{\min} = 1671.238$, with $\Delta\text{AIC} = -12.996$ and $\Delta\text{BIC} = -2.073$, again suggesting a moderate to strong preference over ΛCDM . For CC+PPS+BAO₁ and CC+PPS+DESI DR1, the $f(T, T_G)$ model records χ^2_{\min} values of 1676.329 and 1670.364, respectively, with ΔAIC values of -10.992 and -10.981, and ΔBIC values of -0.054 and -0.055. These results indicate a moderate preference for the $f(T, T_G)$ model based on AIC, while BIC shows a marginal difference, reflecting the penalty for additional free parameters in the modified gravity model compared to three parameters of the ΛCDM . Overall, the consistently negative ΔAIC and ΔBIC values across all datasets highlight the competitive performance of the $f(T, T_G)$ model, positioning it as a viable alternative to ΛCDM . However, the near-zero ΔBIC values for CC+PPS+BAO₁ and CC+PPS+DESI DR1 suggest that the additional parameters in the $f(T, T_G)$ model may not be strongly justified by the data under the BIC criterion, underscoring the need for further refinement to balance model complexity and fit. In Figure 4, we compare the H_0 values derived from joint analyses (as detailed in Table 1) for both the ΛCDM and $f(T, T_G)$ -gravity models against a range of contemporary measurements. These comparisons are categorized into: i) early-universe observations, including Planck 2018 and the DESI collaboration; and ii) late-time measurements from direct observations of the local Universe, such as Supernovae and H_0 for the Equation of State (SH0ES) [75], H0LiCOW [100], and the Hubble Space Telescope (HST) [101]. Figure 4 highlights the discrepancies in H_0 measurements between early-universe data, late-universe observations, and the theoretical frameworks of ΛCDM and $f(T, T_G)$ -gravity explored in this study. The standard ΛCDM model aligns closely with early-universe measurements, which typically predict a lower H_0 , whereas late-time observations from sources like SH0ES and JWST consistently report higher H_0 values. In contrast, the $f(T, T_G)$ gravity model produces elevated H_0 estimates, indicating a closer alignment with late-time observations, though it does not fully reconcile the ongoing tension in H_0 measurements. The total uncertainty in the Hubble parameter computed, represented in Fig. 4 as $\sigma_{\text{total}} = \sqrt{\sigma_{\text{stat}}^2 + \sigma_{\text{sys}}^2}$. This value integrates the statistical uncertainty σ_{stat} derived from MCMC sampling and the systematic uncertainty σ_{sys} associated with observational datasets.

4 Perturbations and stability

In this section, we investigate the stability conditions of cosmological solutions under linear, isotropic, and homogeneous perturbations within the framework of $f(T, T_G)$ gravity. We derive the general perturbation equations for a spatially flat FLRW Universe and apply them to analyze both de Sitter and power-law cosmological solutions.

We consider a general ansatz for the Hubble parameter, given by

$$H(t) = \bar{H}(t), \quad (4.1)$$

Hubble Constant (H_0) Measurements Comparison

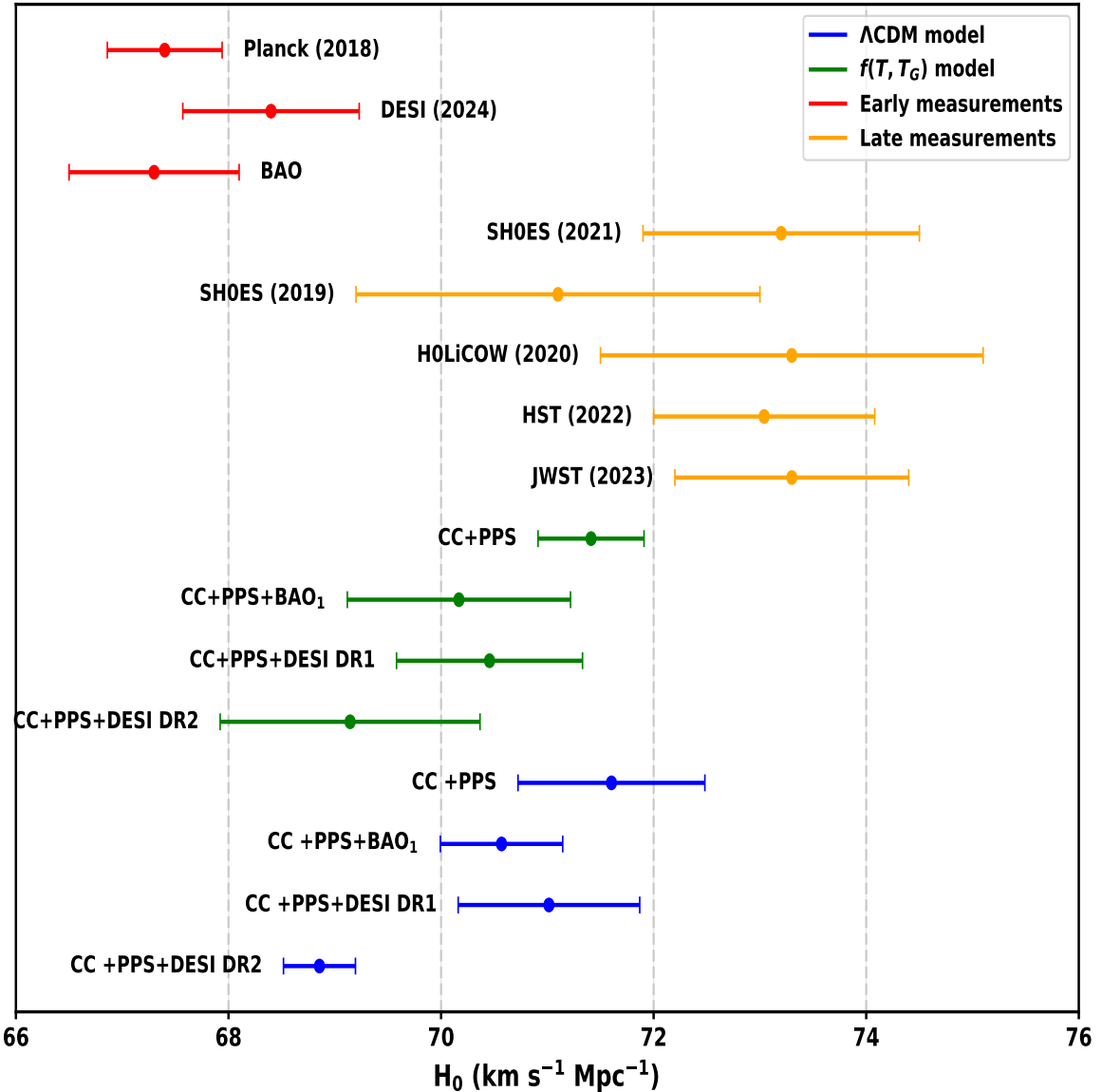


Figure 4. A whisker plot illustrating the Hubble constant (H_0) parameter, highlighting discrepancies between early-time and late-time measurements, Λ CDM and $f(T, T_G)$ models.

which satisfies the modified field equations of motion in $f(T, T_G)$ gravity. Based on this Hubble function, the torsion scalar T and the Gauss-Bonnet invariant T_G are expressed as

$$\bar{T}(t) = 6\bar{H}^2(t), \quad (4.2)$$

$$\bar{T}_G(t) = 24\bar{H}^2(t)\dot{\bar{H}}(t) + 24\bar{H}^4(t). \quad (4.3)$$

Assuming a specific form of the function $f(T, T_G)$ that yields the cosmological solution

given in equation (4.1), the modified Friedmann equations must satisfy

$$-3\bar{H}^2(3\bar{f}_{T_G} + 2\bar{f}_T) + 3\bar{H}\dot{\bar{f}}_{T_G} - 3\dot{\bar{H}}\bar{f}_{T_G} + \frac{1}{2}\bar{f} = \kappa^2\rho_{m0}, \quad (4.4)$$

where \bar{f}_T and \bar{f}_{T_G} denote partial derivatives of the function f with respect to T and T_G , respectively, evaluated on the background solution.

Additionally, the conservation equation for the matter energy density ρ_{m0} with EoS parameter ω is given by

$$\dot{\bar{\rho}}_m + 3\bar{H}\bar{\rho}_m = 0. \quad (4.5)$$

This setup establishes the groundwork for studying the dynamical behavior and stability of various cosmological models within the $f(T, T_G)$ gravity paradigm.

We define the perturbation for the Hubble parameter and energy density as follows

$$H(t) = \bar{H}(t)(1 + \delta(t)), \quad \rho_m(t) = \bar{\rho}_m(1 + \delta_m(t)), \quad (4.6)$$

where $\delta(t)$ and $\delta_m(t)$ denote the dimensionless perturbations associated with the Hubble rate and the matter overdensity, respectively.

To analyze the dynamics of these perturbations within the linear regime, we perform a Taylor series expansion of the function $f(T, T_G)$ about the background values of the torsion scalar \bar{T} and the Gauss-Bonnet invariant \bar{T}_G , corresponding to the unperturbed solution $H(t) = \bar{H}(t)$. The expansion reads

$$f(T, T_G) = \bar{f} + \bar{f}_T(T - \bar{T}) + \bar{f}_{T_G}(T_G - \bar{T}_G) + \mathcal{O}^2, \quad (4.7)$$

where $\bar{f} = f(\bar{T}, \bar{T}_G)$. The term \mathcal{O}^2 includes second-order and higher-order contributions in T and T_G , which are formally retained but do not contribute to the linearized perturbation dynamics.

Substituting the perturbed expressions from equation (4.6) into the modified FLRW background equation (originally denoted as equation (2.19)), and employing the linear expansion from equation (4.7), we obtain the evolution equation governing the perturbation $\delta(t)$ in the linear approximation

$$c_2\ddot{\delta}(t) + c_1\dot{\delta}(t) + c_0\delta(t) = c_m\delta_m(t), \quad (4.8)$$

where c_0 , c_1 , c_2 , and c_m (as provided in the [Appendix A](#)) are time-dependent coefficients determined by the background solution and the form of $f(T, T_G)$. This formulation allows for a systematic analysis of the stability of the cosmological model under isotropic scalar perturbations in modified gravity theories involving curvature invariants. The matter continuity equation (4.5) yields a second perturbed equation when linearized using the expressions in (4.6)

$$\dot{\delta}_m(t) + 3\bar{H}(t)\delta(t) = 0. \quad (4.9)$$

The stability of any FLRW cosmological solution in $f(T, T_G)$ gravity can therefore be investigated through the coupled system of differential equations (4.8) and (4.9). Given the linear nature of equation (4.8), its general solution naturally decomposes into two physically distinct components:

1. The homogeneous solution $\delta_{hom}(t)$, representing perturbations intrinsic to the gravitational sector and determined by the specific form of the $f(T, T_G)$ Lagrangian.

2. The particular solution $\delta_{\text{part}}(t)$, driven exclusively by the matter density perturbations $\delta_m(t)$.

The complete linear solution consequently takes the form

$$\delta(t) = \delta_{\text{hom}}(t) + \delta_{\text{part}}(t). \quad (4.10)$$

Before analyzing specific cosmological scenarios, we begin with some general considerations regarding the stability equations in modified gravity. On the cosmological FLRW background we have $T = 6H^2 \geq 0$, thus $|T| = T$ and $f(T, T_G)|_{\beta=0} = -(1-\alpha)T$. Therefore, the gravitational part of the action is proportional to $(1-\alpha)T$, which is equivalent to the Hilbert–Einstein action up to an overall constant factor. This implies a rescaling of the effective gravitational coupling,

$$\kappa_{\text{eff}}^2 = \frac{\kappa^2}{1-\alpha} \quad (\alpha \neq 1). \quad (4.11)$$

Consequently, in any expression derived from the Friedmann equations one must replace κ^2 by κ_{eff}^2 when working on the TEGR branch with $\beta = 0$ and $\alpha \neq 0$. In particular, the coefficient c_m in [Appendix A](#) (originally written as $c_m = \kappa^2 \rho_m$) becomes

$$c_m = \kappa_{\text{eff}}^2 \rho_m = \frac{\kappa^2}{1-\alpha} \rho_m. \quad (4.12)$$

Note that the case $\alpha \rightarrow 1$ is singular and corresponds to a vanishing effective gravitational coupling; we therefore assume $\alpha \neq 1$ throughout the analysis. In particular, it is instructive to recover the standard GR limit by setting the gravitational Lagrangian to the Hilbert–Einstein form, $f(T, T_G) = -T$. Under this condition, the perturbation equation [\(4.8\)](#) simplifies significantly and reduces to

$$-18\bar{H}^2 \delta(t) = c_m \delta_m(t), \quad (4.13)$$

which establishes a purely algebraic relationship between the geometric perturbation $\delta(t)$ and the matter overdensity $\delta_m(t)$. This implies that within GR, the complete behavior of perturbations around a cosmological solution is fully determined by the matter sector, and conversely, the evolution of matter can be directly inferred from the geometric perturbation.

By combining the explicit form of the coefficients c_m (given in the [Appendix A](#)) with the fundamental relation [\(4.9\)](#), we can directly establish that

$$\delta(t) = -\frac{1}{6} \delta_m(t) \propto a(t)^{1/2}. \quad (4.14)$$

However, this algebraic relation is generally absent in higher-order theories of gravity such as those involving arbitrary functions $f(T, T_G)$. In such cases, the evolution of scalar perturbations is governed by the coupled system of differential equations [\(4.8\)](#) and [\(4.9\)](#), where the gravitational Lagrangian itself significantly influences the dynamics. These coefficients dictate the nature of the perturbation propagation, potentially introducing rich dynamical features absent in standard GR. This foundational contrast underscores the importance of carefully analyzing the stability equations in the context of modified gravity theories, where perturbations exhibit more intricate and model-dependent behavior.

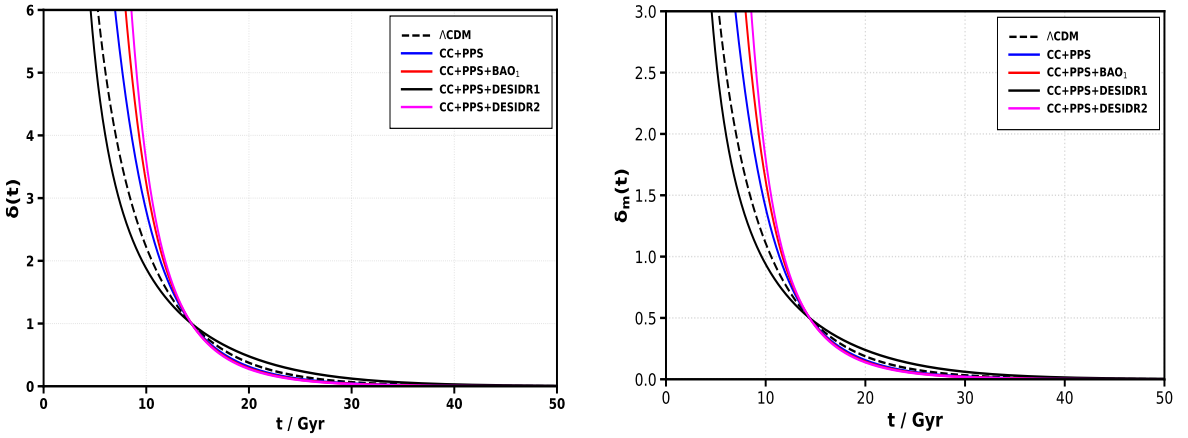


Figure 5. Evolution of the Hubble perturbation parameter $\delta(t)$ (left panel) and the matter perturbation parameter $\delta_m(t)$ (right panel) as a function of cosmic time in the $f(T, T_G)$ gravity model.

Figure 5 illustrates the temporal evolution of the Hubble perturbation parameter $\delta(t)$ (left panel) and the matter perturbation parameter $\delta_m(t)$ (right panel) as functions of cosmic time t in the $f(T, T_G)$ gravity framework. The analysis incorporates the effects of varying the best-fit values of the model parameters, determined through a MCMC parameterization technique. The plots compare four distinct datasets: CC+PPS, CC+PPS+BAO₁, CC+PPS+DESI DR1 and CC+PPS+DESI DR2. The numerical results reveal that both $\delta(t)$ and $\delta_m(t)$ decay rapidly to zero as cosmic time progresses, confirming the stability of the numerical solutions. Fig. 5 illustrates the time evolution of the perturbations. For the Hubble parameter perturbations, the solutions demonstrate stability as they decay monotonically with cosmic time, closely following the behaviour of the Λ CDM model, and eventually vanish at late times. For matter perturbations, the models again show a behaviour similar to Λ CDM, remaining stable and decaying with time, but instead of vanishing completely they asymptotically approach a constant limiting value at late times. Specifically, the Hubble perturbations demonstrate a consistent decay across all datasets, fully stabilizing at late times, indicative of a robust and stable cosmological evolution. Similarly, the matter perturbations mirror this behavior, decaying steadily over time and converging to a limiting value at late times, further reinforcing the stability of the solutions within this gravitational model.

Building on the stability of the $f(T, T_G)$ model confirmed through perturbation analysis, we now summarize its cosmological implications and observational consistency, highlighting its potential as an alternative to Λ CDM.

5 Conclusion

In this study, we investigated the cosmological implications of a specific $f(T, T_G)$ gravity model, which incorporates the torsion scalar T and the teleparallel Gauss-Bonnet invariant T_G . We began by establishing the theoretical framework of $f(T, T_G)$ gravity within a flat FLRW cosmological background, deriving the modified Friedmann equations and exploring the dynamics of cosmic expansion. This model offers a compelling alternative to the standard Λ CDM paradigm by replicating dark energy behavior without invoking a cosmological

constant, thus avoiding associated theoretical challenges such as the fine-tuning and cosmic coincidence problems. We employed a numerical approach to solve the modified Friedmann equations, predicting the redshift evolution of the Hubble parameter $H(z)$. Using Bayesian inference and MCMC techniques, we constrained the model parameters (H_0 , Ω_{m0} , α , β , γ , and M) with high precision, leveraging late-time observational datasets including the CC, PPS, BAO₁ and DESI BAO (DR1 and DR2) measurements. The contour plots in Figure 1 illustrate the 1σ and 2σ uncertainty regions for these parameters, demonstrating the model's consistency across datasets, with H_0 values ranging from $69.144^{+0.450}_{-0.547}$ to $71.411^{+1.214}_{-1.234}$ $\text{km s}^{-1} \text{Mpc}^{-1}$, closely aligning with recent observational bounds. Figure 2 reveals a smooth transition from a decelerating to an accelerating phase, with transition redshifts z_t between 0.834 and 0.846, consistent with observational constraints. The current value of the deceleration parameter q_0 is estimated to be between -0.494 and -0.549 . Similarly, the EoS parameter is observed to range from -0.664 to -0.693 . These findings are consistent with results from Planck 2018 and WMAP combined with CMB analyses, as illustrated in Figure 3.

For the CC+PPS dataset, the $f(T, T_G)$ model achieves a best-fit $\chi^2_{\min} = 1661.412$, with $\Delta\text{AIC} = -17.070$ and $\Delta\text{BIC} = -6.155$. The notably negative values of these criteria indicate a strong statistical preference for the $f(T, T_G)$ scenario compared to the standard ΛCDM model. This is demonstrated in Table 2, which shows consistently negative ΔAIC and ΔBIC values, suggesting a statistically better fit across most cosmological datasets. However, the near-zero ΔBIC for BAO₁ and DESI DR1 highlights the need to refine the model's additional parameters to better balance complexity and fit. Figure 4 reveals a persistent discrepancy in Hubble constant measurements, with the $f(T, T_G)$ gravity model produces H_0 estimates ($69 - 71.5 \text{ km s}^{-1} \text{Mpc}^{-1}$) that are intermediate between early-universe constraints (e.g., Planck 2018: $67.4 \pm 0.5 \text{ km s}^{-1} \text{Mpc}^{-1}$) and late-time observations (e.g., SH0ES: $73.4 \pm 2.0 \text{ km s}^{-1} \text{Mpc}^{-1}$), partially alleviating but not fully resolving the Hubble tension. However, the 3.2σ - 4.1σ tension between Planck and SH0ES persists, indicating that while geometric modifications in $f(T, T_G)$ gravity reduce the Hubble discrepancy, they do not fully resolve it, suggesting the need for additional physics or refined observational calibrations. Additionally, the rapid decay of both Hubble and matter perturbations indicates a stable cosmological evolution, potentially suppressing late-time structure formation compared to ΛCDM . This contrast implies that the model may suppress the growth of large-scale structure, potentially leading to lower matter clustering than observed. Such suppression could be in tension with data from galaxy surveys and weak lensing, which require sufficient structure formation. Therefore, while rapid decay can help alleviate issues like excess power on small scales, it must still be consistent with large-scale structure observations. While the $f(T, T_G)$ model effectively describes late-time cosmic acceleration and aligns with low-redshift observations, its deviations from ΛCDM at higher redshifts suggest it may not fully capture the matter-dominated era. These findings emphasize the need for further investigation into systematic uncertainties or new physics to resolve the H_0 tension and refine our understanding of cosmic expansion. Future work can leverage upcoming observational probes to rigorously test the $f(T, T_G)$ model. The Rubin Observatory's Legacy Survey of Space and Time (LSST) will provide high-precision weak lensing and galaxy clustering data, enabling constraints on the growth rate and clustering amplitude S_8 , which are sensitive to the suppressed perturbation growth of the model.

Acknowledgments

The authors acknowledge that the Ministry of Higher Education, Research, and Innovation (MoHERI) supported this research work through the project BFP/GRG/CBS/24/035. The authors are also thankful to the UoN administration for the continuous support and encouragement for the research work.

Data Availability

There are no associated data with this article. No new data were generated or analysed in support of this research.

Analytical Expressions for Perturbation Coefficients

In this Appendix, we present the explicit analytical expressions for the coefficients appearing in equation (4.8). The coefficients are given below as follows

$$c_0 = -6\bar{H}^2 \left(2 \left(\bar{H}^2 \left(-6\bar{f}_{TT} + 96\bar{f}_{TTg}\dot{\bar{H}} - 4\bar{f}_{Tg} + 648\bar{f}_{TgTg}\dot{\bar{H}}^2 \right) \right. \right. \\ \left. \left. + 12\bar{H}^4 \left(2\dot{\bar{H}} \left(6\bar{f}_{TTTg} + 60\bar{f}_{TTgTg}\dot{\bar{H}} + 65\bar{f}_{TgTg} + 144\bar{f}_{TgTgTg}\dot{\bar{H}}^2 \right) - 5\bar{f}_{TTg} \right) \right. \right. \\ \left. \left. - 96H_0^6 \left(\bar{f}_{TgTg} - 24\dot{\bar{H}} \left(\bar{f}_{TTgTg} + 5\bar{f}_{TgTgTg}\dot{\bar{H}} \right) \right) + 288\bar{H}^5 \ddot{\bar{H}} \left(\bar{f}_{TTgTg} \right. \right. \\ \left. \left. + 6\bar{f}_{TgTgTg}\dot{\bar{H}} \right) - 3\bar{f}_{Tg}\dot{\bar{H}} + 360\bar{H}^3\bar{f}_{TgTg}\ddot{\bar{H}} + 9216\bar{H}^8\bar{f}_{TgTgTg}\dot{\bar{H}} + 2304\bar{H}^7 \right. \\ \left. \times \bar{f}_{TgTg}\ddot{\bar{H}} \right) - 3\bar{f}_T \right), \quad (5.1)$$

$$c_1 = -1224\bar{H}^5 \left(\bar{f}_{TTg} + 17\bar{f}_{TgTg}\dot{\bar{H}} \right) + 24\bar{H}^7 \left(12\dot{\bar{H}} \left(\bar{f}_{TTgTg} + 4\bar{f}_{TgTgTg}\dot{\bar{H}} \right) \right. \\ \left. + 11\bar{f}_{TgTg} \right) - \bar{H}^3\bar{f}_{Tg} + 2304\bar{H}^9\bar{f}_{TgTgTg}\dot{\bar{H}} + 576\bar{H}^8\bar{f}_{TgTgTg}\ddot{\bar{H}}, \quad (5.2)$$

$$c_2 = -864\bar{H}^6\bar{f}_{TgTg}, \quad (5.3)$$

$$c_m = \kappa^2 \bar{\rho}_m. \quad (5.4)$$

6 BAO Distance Measurements from Observational Data

z_{eff}	Value	Observable	Reference
0.81	10.75 ± 0.43	D_A/r_d	[89]
0.38	$10.272 \pm 0.135 \pm 0.074$	D_M/r_d	
0.51	$13.378 \pm 0.156 \pm 0.095$	D_M/r_d	[88]
0.61	$15.449 \pm 0.189 \pm 0.108$	D_M/r_d	
0.698	17.65 ± 0.3	D_M/r_d	[85]
1.48	30.21 ± 0.79	D_M/r_d	[86]
2.3	37.77 ± 2.13	D_M/r_d	[84]
2.4	36.6 ± 1.2	D_M/r_d	[102]
0.15	4.473 ± 0.159	D_V/r_d	[83]
0.44	11.548 ± 0.559	D_V/r_d	
0.6	14.946 ± 0.680	D_V/r_d	[90]
0.73	16.931 ± 0.579	D_V/r_d	
1.52	26.005 ± 0.995	D_V/r_d	[87]
0.698	19.77 ± 0.47	D_H/r_d	[85]
1.48	13.23 ± 0.47	D_H/r_d	[86]
2.3	9.07 ± 0.31	D_H/r_d	[84]
2.4	8.94 ± 0.22	D_H/r_d	[89]
0.38	$12044.07 \pm 251.226 \pm 133.002$	H_{rd} [km/s]	
0.51	$13374.09 \pm 251.226 \pm 147.78$	H_{rd} [km/s]	[88]
0.61	$14378.994 \pm 266.004 \pm 162.558$	H_{rd} [km/s]	

Table 3. Constraints on distance bounds derived from BAO measurements across various observational probes and surveys. The table presents the effective redshift of each measurement, the mean value with its standard deviation, the corresponding observable, and the associated reference.

Tracer	z_{eff}	D_M/r_d	D_H/r_d	r or D_V/r_d
BGS	0.295	-	-	7.93 ± 0.15
LRG1	0.510	13.62 ± 0.25	20.98 ± 0.61	-0.445
LRG2	0.706	16.85 ± 0.32	20.08 ± 0.60	-0.420
LRG3+ELG1	0.930	21.71 ± 0.28	17.88 ± 0.35	-0.389
ELG2	1.317	27.79 ± 0.69	13.82 ± 0.42	-0.444
QSO	1.491	-	-	26.07 ± 0.67
Ly α QSO	2.330	39.71 ± 0.94	8.52 ± 0.17	-0.477

Table 4. Statistical data pertaining to the DESI samples used for the measurements associated with the DESI DR1 BAO. The table presents the effective redshift (z_{eff}) for each observation, along with the corresponding distance ratios: either the correlated pair (D_M/r_d , D_H/r_d) with correlation coefficient r , or the spherically averaged distance D_V/r_d .

References

- [1] SUPERNOVA SEARCH TEAM collaboration, *Observational evidence from supernovae for an accelerating universe and a cosmological constant*, *Astron. J.* **116** (1998) 1009.
- [2] SUPERNOVA COSMOLOGY PROJECT collaboration, *Measurements of Ω and Λ from 42 high redshift supernovae*, *Astrophys. J.* **517** (1999) 565.
- [3] M. Kowalski, D. Rubin, G. Aldering et al., *Improved Cosmological Constraints from New, Old, and Combined Supernova Data Sets*, *Astrophys. J.* **686** (2008) 749.

Tracer	z_{eff}	D_M/r_d	D_H/r_d	r or D_V/r_d
BGS	0.295	-	-	7.942 ± 0.075
LRG1	0.510	13.588 ± 0.167	21.863 ± 0.425	12.720 ± 0.099
LRG2	0.706	17.351 ± 0.177	19.455 ± 0.330	16.050 ± 0.110
LRG3+ELG1	0.934	21.576 ± 0.152	17.641 ± 0.193	19.721 ± 0.091
ELG2	1.321	27.601 ± 0.318	14.176 ± 0.221	24.252 ± 0.174
QSO	1.484	30.512 ± 0.760	12.817 ± 0.516	26.055 ± 0.398
Lya	2.330	38.988 ± 0.531	8.632 ± 0.101	31.267 ± 0.256
LRG3	0.922	21.648 ± 0.178	17.577 ± 0.213	19.656 ± 0.105
ELG1	0.955	21.707 ± 0.335	17.803 ± 0.297	20.008 ± 0.183

Table 5. Statistical data pertaining to the DESI samples used for the measurements associated with the DESI DR2 BAO. The table presents the effective redshift (z_{eff}) for each observation, along with the corresponding distance ratios: either the correlated pair (D_M/r_d , D_H/r_d) with correlation coefficient r , or the spherically averaged distance D_V/r_d .

- [4] P.A.R. Ade, N. Aghanim, M. Arnaud et al., *Planck 2015 results*, *Astron. Astrophys.* **594** (2016) A13.
- [5] N. Jarosik, C.L. Bennett, J. Dunkley et al., *SEVEN-YEAR WILKINSON MICROWAVE ANISOTROPY PROBE (WMAP*) OBSERVATIONS: SKY MAPS, SYSTEMATIC ERRORS, AND BASIC RESULTS*, *Astrophys. J. Supp. Ser.* **192** (2011) 14.
- [6] E. Komatsu, J. Dunkley, M.R. Nolta et al., *FIVE-YEAR WILKINSON MICROWAVE ANISOTROPY PROBE* OBSERVATIONS: COSMOLOGICAL INTERPRETATION*, *Astrophys. J. Supp. Ser.* **180** (2009) 330.
- [7] J. Benjamin, C. Heymans, E. Semboloni et al., *Cosmological constraints from the 100-deg² weak-lensing survey*, *Mon. Not. R. Astron. Soc.* **381** (2007) 702.
- [8] L. Fu, E. Semboloni, H. Hoekstra et al., *Very weak lensing in the CFHTLS wide: cosmology from cosmic shear in the linear regime*, *Astron. Astrophys.* **479** (2008) 9.
- [9] L. Amendola, M. Kunz and D. Sapone, *Measuring the dark side (with weak lensing)*, *J. Cosmol. Astropart. Phys.* **2008** (2008) 013.
- [10] M. Tegmark, M.A. Strauss, M.R. Blanton et al., *Cosmological parameters from SDSS and WMAP*, *Phys. Rev. D* **69** (2004) 103501.
- [11] S. Cole, W.J. Percival, J.A. Peacock et al., *The 2dF Galaxy Redshift Survey: power-spectrum analysis of the final data set and cosmological implications*, *Mon. Not. R. Astron. Soc.* **362** (2005) 505.
- [12] D.J. Eisenstein, I. Zehavi, D.W. Hogg et al., *Detection of the Baryon Acoustic Peak in the Large-Scale Correlation Function of SDSS Luminous Red Galaxies*, *Astrophys. J.* **633** (2005) 560.
- [13] W.J. Percival, B.A. Reid, D.J. Eisenstein et al., *Baryon acoustic oscillations in the Sloan Digital Sky Survey Data Release 7 galaxy sample*, *Mon. Not. Roy. Astron. Soc.* **401** (2010) 2148.
- [14] C. Blake, S. Brough, M. Colless et al., *The WiggleZ Dark Energy Survey: joint measurements of the expansion and growth history at $z < 1$* , *Mon. Not. Roy. Astron. Soc.* **425** (2012) 405.
- [15] A.J. Bunker, S. Wilkins, R.S. Ellis et al., *The contribution of high-redshift galaxies to cosmic reionization: new results from deep WFC3 imaging of the Hubble Ultra Deep Field*, *Mon. Not. R. Astron. Soc.* **409** (2010) 855.

[16] P.J.E. Peebles and B. Ratra, *The Cosmological Constant and Dark Energy*, *Rev. Mod. Phys.* **75** (2003) 559.

[17] S. Weinberg, *The Cosmological Constant Problem*, *Rev. Mod. Phys.* **61** (1989) 1.

[18] S.M. Carroll, *The Cosmological Constant*, *Living Rev. Rel.* **4** (2001) 1.

[19] A.H. Wright et al., *KiDS-Legacy: Cosmological Constraints from the Final Dataset*, *arXiv e-prints* (2025) [[2503.19441](https://arxiv.org/abs/2503.19441)].

[20] L. Perivolaropoulos and F. Skara, *Challenges for Λ CDM: an update*, *New Astron. Rev.* **95** (2022) 101659.

[21] E. Di Valentino, J.L. Said, A. Riess et al., *The CosmoVerse White Paper: Addressing observational tensions in cosmology with systematics and fundamental physics*, *arXiv: 2504.01669 [astro-ph.CO]* (2025) .

[22] S. Tsujikawa, *Lectures on Cosmology*, *Lect. Notes Phys.* **800** (2010) 99.

[23] R.R. Caldwell, R. Dave and P.J. Steinhardt, *Cosmological Imprint of an Energy Component with General Equation of State*, *Phys. Rev. Lett.* **80** (1998) 1582.

[24] E.J. Copeland, M. Sami and S. Tsujikawa, *Dynamics of dark energy*, *Int. J. Mod. Phys. D* **15** (2006) 1753.

[25] T. Padmanabhan, *Accelerated expansion of the universe driven by tachyonic matter*, *Phys. Rev. D* **66** (2002) 021301.

[26] J.A. Frieman, M.S. Turner and D. Huterer, *Dark Energy and the Accelerating Universe*, *Annu. Rev. Astron. Astrophys.* **46** (2008) 385.

[27] D.H. Weinberg, M.J. Mortonson, D.J. Eisenstein et al., *Observational probes of cosmic acceleration*, *Phys. Rep.* **530** (2013) 87.

[28] A. Adame, J. Aguilar, S. Ahlen et al., *DESI 2024 VI: cosmological constraints from the measurements of baryon acoustic oscillations*, *J. Cosmol. Astropart. Phys.* **2025** (2025) 021.

[29] A. Lue, *The phenomenology of dvali–gabadadze–porrati cosmologies*, *Phys. Rep.* **423** (2006) 1.

[30] S. Nojiri and S.D. Odintsov, *Introduction to Modified Gravity and Gravitational Alternative for Dark Energy*, *Int. J. Geom. Methods Mod. Phys.* **04** (2007) 115.

[31] A. Starobinsky, *A new type of isotropic cosmological models without singularity*, *Phys. Lett. B* **91** (1980) 99.

[32] A.D. Felice and S. Tsujikawa, *$f(R)$ Theories*, *Living Rev. Rel.* **13** (2010) 3.

[33] P.G.S. Fernandes, P. Carrilho, T. Clifton et al., *The 4D Einstein–Gauss–Bonnet theory of gravity: a review*, *Class. Quant. Grav.* **39** (2022) 063001.

[34] D. Lovelock, *The Einstein Tensor and Its Generalizations*, *J. Math. Phys.* **12** (1971) 498.

[35] Y.-F. Cai, S. Capozziello, M.D. Laurentis et al., *$f(T)$ teleparallel gravity and cosmology*, *Rept. Prog. Phys.* **79** (2016) 106901.

[36] L. Heisenberg, *Review on $f(Q)$ Gravity*, *Phys. Rep.* **1066** (2023) 1.

[37] S. Vagnozzi, F. Pacucci and A. Loeb, *Implications for the hubble tension from the ages of the oldest astrophysical objects*, *J. High Energy Astrophys.* **36** (2022) 27.

[38] S. Vagnozzi, *New physics in light of the H_0 tension: An alternative view*, *Phys. Rev. D* **102** (2020) 023518.

[39] A. Ilyas, M. Zhu, Y. Zheng et al., *DHOST bounce*, *J. Cosmol. Astropart. Phys.* **09** (2020) 002.

[40] S.V. Lohakare, S. Niyogi and B. Mishra, *Cosmology in modified $f(\mathcal{G})$ gravity: a late-time cosmic phenomena*, *Mon. Not. R. Astron. Soc.* **535** (2024) 1136.

[41] S.V. Lohakare and B. Mishra, *Stability of $f(Q, B)$ Gravity via Dynamical System Approach: A Comprehensive Bayesian Statistical Analysis*, *Astrophys. J.* **978** (2024) 26.

[42] K. Bamba, S. Capozziello, S. Nojiri et al., *Dark energy cosmology: the equivalent description via different theoretical models and cosmography tests*, *Astrophys. Space Sci.* **342** (2012) 155.

[43] D.G. Boulware and S. Deser, *String-generated gravity models*, *Phys. Rev. Lett.* **55** (1985) 2656.

[44] J.T. Wheeler, *Symmetric solutions to the gauss-bonnet extended einstein equations*, *Nuclear Phys. B* **268** (1986) 737.

[45] I. Antoniadis, J. Rizos and K. Tamvakis, *Singularity-free cosmological solutions of the superstring effective action*, *Nuclear Phys. B* **415** (1994) 497.

[46] S. Nojiri, S.D. Odintsov and M. Sasaki, *Gauss-Bonnet dark energy*, *Phys. Rev. D* **71** (2005) 123509.

[47] G. Kofinas and E.N. Saridakis, *Teleparallel equivalent of Gauss-Bonnet gravity and its modifications*, *Phys. Rev. D* **90** (2014) 084044.

[48] G. Kofinas and E. N. Saridakis, *Cosmological applications of $F(T, T_G)$ gravity*, *Phys. Rev. D* **90** (2014) 084045.

[49] T. Harko, F.S. Lobo, G. Otalora et al., *$f(T, T)$ gravity and cosmology*, *J. Cosmol. Astropart. Phys.* **2014** (2014) 021.

[50] L.K. Duchaniya and B. Mishra, *Late time phenomena in $f(T, T)$ gravity framework: role of H_0 priors*, *Eur. Phys. J. C* **85** (2025) 488.

[51] T. Harko, F.S. Lobo, G. Otalora et al., *Nonminimal torsion-matter coupling extension of $f(T)$ gravity*, *Phys. Rev. D* **89** (2014) 124036.

[52] S. Chattopadhyay, D. Momeni and R. Myrzakulov, *Pilgrim dark energy in $f(T, T_G)$ cosmology*, *Astrophys. Space Sci.* **2014** (2014) 279.

[53] S. Capozziello, M. De Laurentis and K.F. Dialektopoulos, *Noether symmetries in Gauss-Bonnet-teleparallel cosmology*, *Eur. Phys. J. C* **76** (2016) 629.

[54] R. Aldrovandi and J.G. Pereira, *Teleparallel Gravity: An Introduction*, Springer (2013), [10.1007/978-94-007-5143-9](https://doi.org/10.1007/978-94-007-5143-9).

[55] J.W. Maluf, *Hamiltonian formulation of the teleparallel description of general relativity*, *J. Math. Phys.* **35** (1994) 335.

[56] H.I. Arcos and J.G. Pereira, *Torsion gravity: A Reappraisal*, *Int. J. Mod. Phys. D* **13** (2004) 2193.

[57] G. Kofinas, G. Leon and E.N. Saridakis, *Dynamical behavior in $f(T, T_G)$ cosmology*, *Class. Quant. Grav.* **31** (2014) 175011.

[58] S.V. Lohakare et al., *Analyzing the geometrical and dynamical parameters of modified Teleparallel-Gauss-Bonnet model*, *Phys. Dark Univ.* **39** (2023) 101164.

[59] E.J. Copeland, *Exponential potentials and cosmological scaling solutions*, *Phys. Rev. D* **57** (1998) 4686.

[60] P.G. Ferreira and M. Joyce, *Structure formation with a self-tuning scalar field*, *Phys. Rev. Lett.* **79** (1997) 4740.

[61] X.-M. Chen, Y. Gong and E.N. Saridakis, *Phase-space analysis of interacting phantom cosmology*, *J. Cosmol. Astropart. Phys.* **2009** (2009) 001.

[62] A. Lewis, *GetDist: a Python package for analysing Monte Carlo samples*, *arXiv: 1910.13970* (2019) [[1910.13970](https://arxiv.org/abs/1910.13970)].

[63] D. Foreman-Mackey et al., *emcee: The mcmc hammer*, *Publ. Astron. Soc. Pac.* **125** (2013) 306.

[64] M. Moresco, L. Amati, L. Amendola et al., *Unveiling the Universe with emerging cosmological probes*, *Living Rev. Rel.* **25** (2022) 6.

[65] D. Brout, D. Scolnic, B. Popovic et al., *The Pantheon+ Analysis: Cosmological Constraints*, *Astrophys. J.* **938** (2022) 110.

[66] D. Scolnic, D. Brout, A. Carr et al., *The Pantheon+ Analysis: The Full Data Set and Light-curve Release*, *Astrophys. J.* **938** (2022) 113.

[67] DESI DR2 RESULTS II collaboration, *DESI DR2 Results II: Measurements of Baryon Acoustic Oscillations and Cosmological Constraints*, *arXiv: 2503.14738* (2025) .

[68] R. D'Agostino and O. Luongo, *Growth of matter perturbations in nonminimal teleparallel dark energy*, *Phys. Rev. D* **98** (2018) 124013.

[69] R. D'Agostino, *Holographic dark energy from nonadditive entropy: Cosmological perturbations and observational constraints*, *Phys. Rev. D* **99** (2019) 103524.

[70] S.V. Lohakare, K. Rathore and B. Mishra, *Observational constrained $F(R, G)$ gravity cosmological model and the dynamical system analysis*, *Class. Quant. Grav.* **40** (2023) 215009.

[71] R. Jimenez and A. Loeb, *Constraining Cosmological Parameters Based on Relative Galaxy Ages*, *Astrophys. J.* **573** (2002) 37.

[72] M. Moresco, A. Cimatti, R. Jimenez et al., *Improved constraints on the expansion rate of the Universe up to $z \sim 1.1$ from the spectroscopic evolution of cosmic chronometers*, *J. Cosmol. Astropart. Phys.* **2012** (2012) 006.

[73] M. Moresco, *Raising the bar: new constraints on the Hubble parameter with cosmic chronometers at $z \sim 2$* , *Mon. Not. Roy. Astron. Soc.: Lett.* **450** (2015) L16.

[74] M. Moresco, L. Pozzetti, A. Cimatti et al., *A 6% measurement of the Hubble parameter at $z \sim 0.45$: direct evidence of the epoch of cosmic re-acceleration*, *J. Cosmol. Astropart. Phys.* **2016** (2016) 014.

[75] A.G. Riess, W. Yuan, L.M. Macri et al., *A Comprehensive Measurement of the Local Value of the Hubble Constant with $1 \text{ km s}^{-1} \text{ Mpc}^{-1}$ Uncertainty from the Hubble Space Telescope and the SH0ES Team*, *Astrophys. J. Lett.* **934** (2022) L7.

[76] A.T. Chantada, S.J. Landau, P. Protopapas et al., *Cosmology-informed neural networks to solve the background dynamics of the Universe*, *Phys. Rev. D* **107** (2023) 063523.

[77] D. Camarena and V. Marra, *Local determination of the Hubble constant and the deceleration parameter*, *Phys. Rev. Res.* **2** (2020) 013028.

[78] A. Conley, J. Guy, M. Sullivan et al., *Supernova Constraints and Systematic Uncertainties From the First Three Years of the Supernova Legacy Survey*, *Astrophys. J. Supp. Ser.* **192** (2011) 1.

[79] L. Perivolaropoulos, *Hubble tension or distance ladder crisis?*, *Phys. Rev. D* **110** (2024) 123518.

[80] W.L. Freedman, B.F. Madore, I.S. Jang et al., *Status Report on the Chicago-Carnegie Hubble Program (CCHP): Measurement of the Hubble Constant Using the Hubble and James Webb Space Telescopes*, *arXiv: 2408.06153 [astro-ph.CO]* (2025) .

[81] DES COLLABORATION collaboration, *Dark energy survey year 3 results: Cosmological constraints from galaxy clustering and weak lensing*, *Phys. Rev. D* **105** (2022) 023520.

[82] M. Asgari, C.-A. Lin, B. Joachimi et al., *KiDS-1000 cosmology: Cosmic shear constraints and comparison between two point statistics*, *Astron. Astrophys.* **645** (2021) A104.

[83] A.J. Ross, L. Samushia, C. Howlett et al., *The clustering of the SDSS DR7 main Galaxy sample – I. A 4 per cent distance measure at $z=0.15$* , *Mon. Not. R. Astron. Soc.* **449** (2015) 835.

[84] J.E. Bautista, N.G. Busca, J. Guy et al., *Measurement of baryon acoustic oscillation correlations at $z = 2.3$ with SDSS DR12 Ly α – Forests*, *Astron. Astrophys.* **603** (2017) A12.

[85] J.E. Bautista, R. Paviot, M. Vargas Magaña et al., *The completed SDSS-IV extended Baryon Oscillation Spectroscopic Survey: measurement of the BAO and growth rate of structure of the luminous red galaxy sample from the anisotropic correlation function between redshifts 0.6 and 1*, *Mon. Not. R. Astron. Soc.* **500** (2020) 736.

[86] R. Neveux, E. Burtin, A. de Mattia et al., *The completed SDSS-IV extended Baryon Oscillation Spectroscopic Survey: BAO and RSD measurements from the anisotropic power spectrum of the quasar sample between redshift 0.8 and 2.2*, *Mon. Not. R. Astron. Soc.* **499** (2020) 210.

[87] M. Ata, F. Baumgarten, J. Bautista et al., *The clustering of the SDSS-IV extended Baryon Oscillation Spectroscopic Survey DR14 quasar sample: first measurement of baryon acoustic oscillations between redshift 0.8 and 2.2*, *Mon. Not. R. Astron. Soc.* **473** (2017) 4773.

[88] S. Alam, M. Ata, S. Bailey et al., *The clustering of galaxies in the completed SDSS-III Baryon Oscillation Spectroscopic Survey: cosmological analysis of the DR12 galaxy sample*, *Mon. Not. Roy. Astron. Soc.* **470** (2017) 2617.

[89] T.M.C. Abbott, F.B. Abdalla, A. Alarcon et al., *Dark Energy Survey Year 1 results: measurement of the baryon acoustic oscillation scale in the distribution of galaxies to redshift 1*, *Mon. Not. R. Astron. Soc.* **483** (2018) 4866.

[90] E.A. Kazin, J. Koda, C. Blake et al., *The WiggleZ Dark Energy Survey: improved distance measurements to $z=1$ with reconstruction of the baryonic acoustic feature*, *Mon. Not. R. Astron. Soc.* **441** (2014) 3524.

[91] C. Gruber and O. Luongo, *Cosmographic analysis of the equation of state of the universe through padé approximations*, *Phys. Rev. D* **89** (2014) 103506.

[92] N.G. Busca, T. Delubac, J. Rich et al., *Baryon acoustic oscillations in the Ly α forest of BOSS quasars*, *Astron. Astrophys.* **552** (2013) A96.

[93] O. Farooq and B. Ratra, *Hubble parameter measurement constraints on the cosmological deceleration-acceleration transition redshift*, *Astrophys. J. Lett.* **766** (2013) L7.

[94] S. Capozziello, O. Farooq, O. Luongo et al., *Cosmographic bounds on the cosmological deceleration-acceleration transition redshift in $f(\mathcal{R})$ gravity*, *Phys. Rev. D* **90** (2014) 044016.

[95] Y. Yang and Y. Gong, *The evidence of cosmic acceleration and observational constraints*, *J. Cosmol. Astropart. Phys.* **2020** (2020) 059.

[96] PLANCK 2018 RESULTS collaboration, *Planck 2018 results. VI. Cosmological parameters*, *Astron. Astrophys.* **652** (2021) C4.

[97] G. Hinshaw, D. Larson, E. Komatsu et al., *Nine-year Wilkinson Microwave Anisotropy Probe (WMAP) Observations: Cosmological Parameter Results*, *Astrophys. J. Supp. Ser.* **208** (2013) 19.

[98] H. Akaike, *A new look at the statistical model identification*, *IEEE Trans. Autom. Control* **19** (1974) 716.

[99] G. Schwarz, *Estimating the Dimension of a Model*, *Ann. Stat.* **6** (1978) 461.

[100] K.C. Wong, S.H. Suyu, G.C.-F. Chen et al., *H0LiCOW – XIII. A 2.4 per cent measurement of H_0 from lensed quasars: 5.3σ tension between early- and late-Universe probes*, *Mon. Not. Roy. Astron. Soc.* **498** (2020) 1420.

- [101] G.C.-F. Chen, S.H. Suyu, K.C. Wong et al., *SHARP-III. First use of adaptive-optics imaging to constrain cosmology with gravitational lens time delays*, *Mon. Not. Roy. Astron. Soc.* **462** (2016) 3457.
- [102] H. du Mas des Bourboux, J.-M. Le Goff, M. Blomqvist et al., *Baryon acoustic oscillations from the complete SDSS-III Ly α -quasar cross-correlation function at $z = 2.4$* , *Astron. Astrophys.* **608** (2017) A130.